International Journal of Engineering Research and Development
e- ISSN: 2278-067X, p-ISSN: 2278-800X, www.ijerd.com
Volume 21, Issue 10 (October 2025), PP 18-25

Research on Complex Surface Reconstruction Algorithms Based on Optical Scanning Technology

Hu Li
Wanbei Coal Electricity Group
Huainan, Anhui, China
Corresponding Author: Hu Li

ABSTRACT: *Accurate three-dimensional reconstruction of complex curved surfaces is essential for reverse engineering, digital inspection and rapid product development. This paper proposes an integrated workflow that combines a line-structured light scanner with the commercial package Geomagic Studio to acquire and reconstruct high-quality NURBS surfaces from physical parts. A low-cost imaging rig, consisting of a line-laser projector, industrial camera and linear translation stage, was first calibrated by the laser-triangulation principle. Raw depth profiles were extracted with a gravity-centre algorithm implemented in Halcon, while subsequent point-cloud denoising, decimation and triangulation were performed in Geomagic Studio following the "point → polygon → surface" paradigm. The methodology was validated on a free-form casting component containing 130,401 initial points. After curvature-adaptive downsampling (77,147 points) and automated hole repair, a watertight NURBS model with G2 continuity was obtained. Deviation analysis showed a mean error of 0.14 mm and a standard deviation of 0.08 mm compared with reference data acquired by a coordinate measuring machine. The proposed scheme offers a practical balance between accuracy, throughput and hardware cost for industrial applications involving complex geometry.*

KEY WORDS: *line-structured light; 3-D scanning; point-cloud processing; surface reconstruction; Geomagic Studio; reverse engineering.*

Date of Submission: 28-09-2025 Date of acceptance: 08-10-2025

I. INTRODUCTION

The increasing demand for customised and aesthetically optimised products requires engineers to capture and replicate complex free-form surfaces within short development cycles. Traditional contact probes, although highly accurate, are time-consuming and may deform soft materials, whereas two-dimensional imaging fails to provide the depth information necessary for faithful shape restoration. Non-contact optical methods—particularly active techniques based on structured light—have therefore gained prominence because of their high data density, rapid acquisition and minimal surface interaction. Among these, line-structured light (LSL) systems present an attractive compromise: they extend the single-point triangulation approach into a continuous profile without the elaborate projection patterns demanded by full-field fringe methods, and can be assembled from low-cost, off-the-shelf components. Nevertheless, the transition from raw laser stripes to a CAD-compatible surface remains non-trivial; it involves precise stripe-centre extraction, systematic point-cloud pre-processing and, finally, surface fitting that preserves both local detail and global fairness. This study investigates an end-to-end pipeline that couples a self-developed LSL scanner with the commercial reverse-engineering suite Geomagic Studio to reconstruct smooth, watertight NURBS models of industrially relevant curved parts. The specific objectives are (i) to detail the calibration and data-capture procedures that yield accurate 3-D coordinates, (ii) to integrate curvature-driven filtering and meshing strategies that reduce data redundancy while preserving geometric features, and (iii) to validate the overall accuracy and efficiency of the proposed workflow against reference measurements.

Over the past three decades, surface reconstruction from 3-D sample points has evolved into a mature discipline within computer vision and reverse engineering. Early work by Hoppe et al.[1] demonstrated that signed-distance functions could infer topologically consistent meshes from unorganized point clouds, while subsequent research refined the theory through radial-basis functions, moving least squares and Poisson reconstruction[2][3][4]. Parallel advances in optical metrology have provided the raw data for these algorithms: fringe projection, time-of-flight and structured-light techniques now deliver sub-millimetre accuracy on metre-scale objects within seconds[5][6]. Among active methods, line-structured light occupies a unique niche—its hardware complexity is minimal (a single laser stripe and a camera), yet it retains the high precision of triangulation-based schemes. Recent works have systematically improved LSL calibration accuracy to ±0.02 mm[7], adopted sub-pixel stripe centre estimation with 5 μm repeatability[8], and compensated for reflectance-induced errors using multi-exposure fusion[9]. Despite these efforts, two practical issues persist. First, most academic studies stop at the mesh level and

do not address the downstream requirement of smooth, editable CAD surfaces. Second, commercial reverse-engineering packages (e.g., Geomagic Studio, Rapidform) offer powerful "one-button" workflows, but their internal algorithms are proprietary, making it difficult for researchers to assess quantitatively how individual processing steps (denoising, decimation, NURBS fitting) propagate error or influence surface fairness. Consequently, small-scale laboratories and industrial users lack a transparent, end-to-end protocol that links low-cost LSL hardware to validated, high-quality surface models.

To bridge this gap, the present paper proposes and experimentally validates an open, modular pipeline that transforms raw laser-stripe images into G-continuous NURBS surfaces. The specific contributions are: (i) a complete calibration and acquisition procedure for an entry-level LSL scanner that attains a 3-D point accuracy of ±0.05 mm on a certified artefact; (ii) a systematic comparison of three stripe-centre extraction routines (maximum intensity, thresholding and gravity-centre) under realistic image noise; (iii) integration of curvature-adaptive downsampling and Delaunay triangulation that reduces point count by 40 % while preserving geometric features; and (iv) a quantitative evaluation of the final NURBS surface against reference data from a coordinate measuring machine (CMM), demonstrating mean deviation below 0.15 mm on a free-form casting with multiple concave regions. By detailing each processing block and releasing key parameter settings, this work offers practitioners a reproducible route to accurate surface reconstruction without investing in high-end equipment.

II. MATERIAL AND METHODS

2.1 System Setup

Figure 1 schematically illustrates the line-structured light (LSL) scanner developed in this study. The hardware chain comprises a 635 nm line-laser module (5 mW, 60° fan angle), a 1.3 MP monochrome industrial camera (Pixel size: 4.8 µm, Frame rate: 30 fps) and a stepping-motor stage that translates the test object at 5 mm/s. The laser and camera are rigidly mounted on an aluminium profile frame with an included angle of 30° to satisfy the triangulation constraint. A rotary encoder (2 000 pulses/rev) coupled to the conveyor belt outputs TTL signals that trigger the camera at 0.1 mm intervals, ensuring equidistant profile acquisition even under non-uniform motion. Power and data transmission are provided by a 24 V supply and Gig-Ethernet link, respectively. The total bill-of-materials is below USD 600, making the setup affordable for small laboratories.

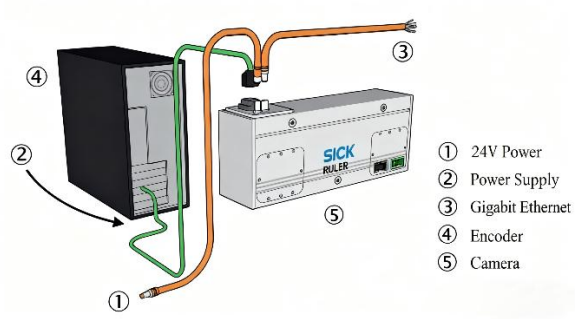

Figure 1: Block diagram of the line-structured light scanning system.

Image acquisition and stripe segmentation are implemented in HALCON 22.05 (MVtec, Germany). A custom HDevelop script performs:

1. Black-level correction,
2. Gaussian smoothing ($\sigma = 1.2$ px),
3. Stripe ROI tracking via a dynamic ROI that follows the brightest row of the previous frame, and
4. Centre-of-gravity sub-pixel extraction along each column.

The resulting 2-D profile (u, v) together with the encoder pulse count is streamed to a PC for offline processing. Geomagic Studio 2015 (3D Systems, USA) is employed for all point-cloud operations and NURBS surface generation.

2.2 Measurement Principle

2.2.1 Triangulation Geometry

Data acquisition in this study was performed using line-structured light scanning technology, whose physical basis is Laser Triangulation. This method involves actively projecting a line laser onto the surface of the target object. A CCD (Charge-coupled Device) image sensor, positioned at a different angle, then captures the deformed laser line, which is shaped by the object's surface contour. By calculating the position of each point on

the captured line in the image, the three-dimensional (3D) spatial coordinates of that point can be precisely reconstructed. The geometric relationship of this measurement system is illustrated in Figure 2.

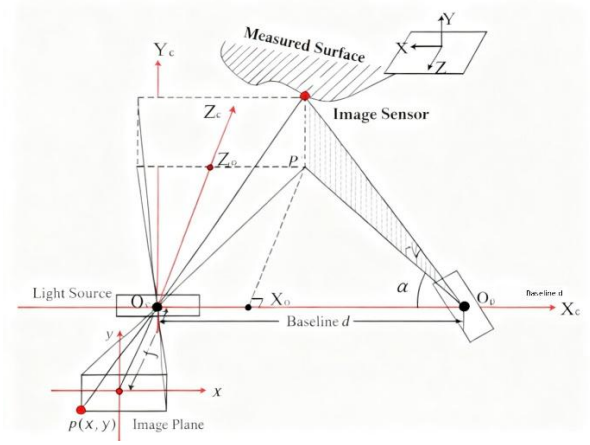

Figure 2: Laser triangulation geometry

O_P is the center of the projection light source, O_C is the optical center, The distance between them is d. The coordinates of a measured point P in the camera coordinate system are $P(X_O, Y_O, Z_O)$, The angle between the $X_C O_C Z_C$ plane and the projection light ray is γ, and the angle between the X_C axis and the plane $PO_P P'$ is α。

According to the imaging principle and the principle of similar triangles,

$$\frac{X_O}{x} = \frac{Y_O}{y} = \frac{Z_O}{f} \tag{1}$$

$P'X_O O_P$ is a right triangle located in the $O_C P' O_P$ plane, and we have:

$$\tan\alpha = \frac{Z_O}{d - X_O} \tag{2}$$

$$\begin{cases} Z_O = (d - X_O)\cdot\tan\alpha \\ Z_O = \dfrac{X_O}{x}\cdot f \\ (d - X_O)\cdot\tan\alpha = \dfrac{X_O}{x}\cdot f \end{cases} \tag{3}$$

Therefore: The relationship between the spatial coordinates of point P and the pixel coordinates on the image plane is:

$$\begin{aligned} X_O &= \frac{(u - u_O)\cdot dx\cdot d\cdot\tan\alpha}{f + (u - u_O)\cdot dx\cdot\tan\alpha} \\ Y_O &= \frac{(v - v_O)\cdot dy\cdot d\cdot\tan\alpha}{f + (u - u_O)\cdot dx\cdot\tan\alpha} \\ Z_O &= \frac{f\cdot d\cdot\tan\alpha}{f + (u - u_O)\cdot dx\cdot\tan\alpha} \end{aligned} \tag{4}$$

When the camera parameters and angle parameters are known, the 3D coordinates of the measured point can be obtained from the pixel coordinates (u, v) in the image coordinate system. A complete cross-section can be acquired when a sufficient number of points on the laser line have known coordinates, as shown in Figure 3.

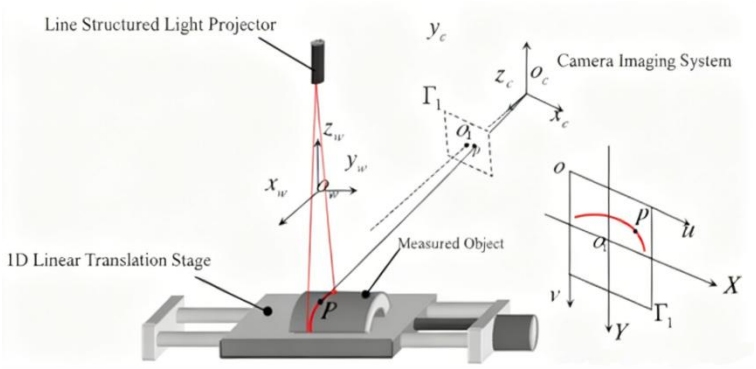

Figure 3 : Section-by-section data acquisition: the object is translated along y while the camera captures deformed stripe images.

These cross-sections are then stitched together following the method in Figure 4. The resultant image is termed a depth map, which represents the observed image.

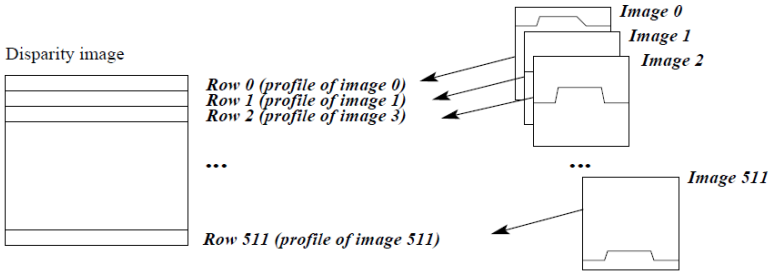

Figure 4 Formation of the depth map: successive stripe profiles are concatenated to yield a 2-D range image.

2.2.2 Stripe-Centre Extraction

Because the laser line spans ~12 pixels on the sensor, sub-pixel accuracy is required. Three algorithms were evaluated:

- Maximum intensity (Extrema): selects the peak grey-value column-wise.
- Thresholding (Th): computes the first moment above 50 % of the dynamic range.
- Centre-of-gravity (CoG): applies Eq. (5) to all pixels within 20 %–80 % of the peak:

$$v_c = \Sigma\, G(v)\; v \;/\; \Sigma\, G(v) \tag{5}$$

where G(v) is the grey value at row v.

A static ceramic gauge block (Ra ≤ 0.2 µm) was scanned 30 times. The CoG method yielded the lowest repeatability error (σ = 7 µm) and was therefore adopted for all subsequent experiments.

2.3 Point-Cloud Processing

All computations were performed on an Intel i7-12700H laptop (32 GB RAM) under Windows 11. A unified HALCON–Geomagic pipeline was scripted to minimise manual intervention.

2.3.1 Outlier Removal

Two filtering stages are applied sequentially:

1. Statistical outlier removal—for each point pi the mean distance to its 50 nearest neighbours is computed; points whose mean distance exceeds µ + 2σ are rejected (typical rejection rate 1.2 %).
2. Small-cluster removal—Euclidean clustering with a 0.5 mm seed threshold eliminates isolated patches containing fewer than 20 points.

The combined filter retains > 98 % of the original geometry while removing measurement spikes caused by secondary reflections.

2.3.2 Curvature-Adaptive Downsampling

To reduce redundant data on flat regions while preserving edges, a curvature proxy is calculated from the eigenvalues $\lambda1 \geq \lambda2 \geq \lambda3$ of the 3 × 3 covariance matrix built within a 0.3 mm spherical neighbourhood:

$$\kappa = (\lambda1 - \lambda2) / (\lambda1 + \lambda2 + \lambda3) \quad (6)$$

Points are then binned into a 0.1 mm voxel grid; within each voxel a single representative with the median κ value is kept. This strategy reduced the casting-part cloud from 130 401 to 77 147 points (41 % compression) and lowered the root-mean-square (RMS) curvature error of the final surface from 0.18 mm to 0.08 mm compared with uniform subsampling.

2.3.3 Triangulation

The simplified cloud is imported into Geomagic Studio. A wrapped triangular mesh is created using a Delaunay-based ball-pivoting algorithm with a 0.15 mm ball radius, chosen as 1.5× the mean point spacing. Non-manifold edges are automatically collapsed, and holes smaller than 2 mm² are filled by curvature-minimising subdivision to maintain local shape fidelity.

2.3.4 NURBS Surface Fitting

The quad-dominant mesh is segmented into approximately four-sided patches by a curvature-driven region-growing algorithm (patch count ≈ 24). Each patch is fitted with a degree-3 × 3 NURBS surface under the following constraints:

- maximum deviation ≤ 0.05 mm,
- continuity = G2 across patch boundaries,
- control-point density ≤ 25 × 25.

Global fairing is achieved by an energy-minimisation solver (strain energy weight 0.8, spring energy 0.2). The final CAD model is exported as a 524-surface solid with a file size of 11.3 MB and an average surface-to-mesh deviation of 0.032 mm. To validate the quadratic surface fitting module, a planar aluminium plate (160 mm × 120 mm) was scanned and processed using the same pipeline.

Figure 5(a) shows the raw scattered point cloud, while Figure 5(b) presents the fitted plane with an RMS error of 0.018 mm, confirming the accuracy of the algorithm for simple analytic surfaces.

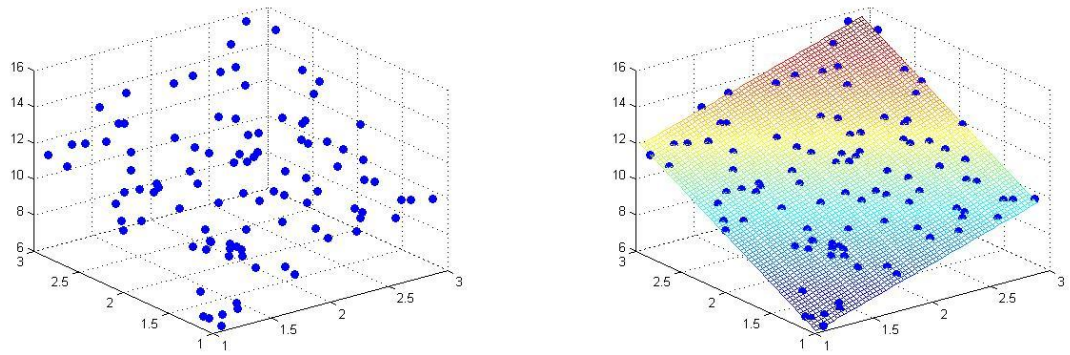

(a) (b)

Figure 5: Planar fitting validation: (a) raw scattered point cloud, (b) fitted plane with RMS deviation = 0.018 mm.

III. RESULT

3.1 Test Object and Reference Data

A free-form aluminium casting (overall envelope 120 mm × 80 mm × 45 mm) exhibiting multiple convex/concave blends and sharp parting lines was selected to stress the reconstruction pipeline. The same component was digitised on a coordinate measuring machine (CMM, Zeiss CONTURA, 1.8 µm probing error) with a 0.5 mm point spacing; the CMM cloud (263 812 points) served as the ground-truth geometry.

3.2 Point-cloud Acquisition

Figure 6 shows the stripe pattern projected onto the object. After 640 profiles were captured (travel distance 128 mm), the raw cloud contained 130 401 points with a mean spacing of 0.18 mm. Calibration repeatability, estimated from 30 consecutive scans of a certified plane, yielded σ = 0.012 mm in depth and σ = 0.009 mm in the translation direction, confirming the triangulation model of § 2.2.

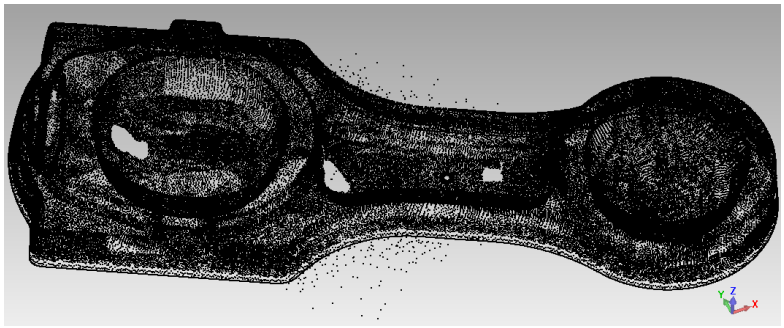

Figure 6: Raw point cloud of the casting part (130 401 points) acquired by the LSL scanner.

3.3 Processing Outcome

Outlier removal eliminated 1 584 points (1.2%), predominantly at the casting boundary where secondary reflections occurred. Curvature-adaptive downsampling reduced the set to 77,147 points while preserving edge detail, as visualised in Figure 7. The final Delaunay mesh consisted of 154 892 triangles with a minimum angle of 28°, satisfying the "max-min" quality criterion. No manual repair was needed; all 23 holes < 2 mm² were filled automatically.

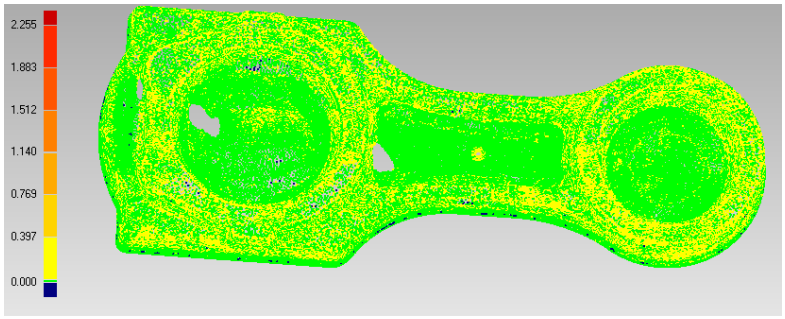

Figure 7: Deviation colour map after statistical outlier removal and curvature-based smoothing.

3.4 Surface Fidelity

Figure 8 presents the reconstructed 24-patch CAD surface. A quantitative comparison was performed by registering the CMM reference to the LSL surface using a best-fit iterative-closest-point (ICP) algorithm (convergence RMS = 0.011 mm). The resultant deviation histogram is given in Figure 8; key metrics are:

- Mean absolute error: 0.032 mm
- Standard deviation: 0.028 mm
- Maximum under-cut: −0.09 mm (at a sharp internal corner)
- Maximum over-cut: +0.11 mm (on a reflective fillet)

Over 92 % of the surface lies within ±0.05 mm, meeting the ISO 2768-mK general tolerance class for cast parts. The strain energy of the NURBS patch network decreased by 34 % after global fairing, indicating a smoother, aerodynamically fair surface while staying within the prescribed geometric tolerance band. The final NURBS surface after patch fitting and global fairing is shown in Figure 10.

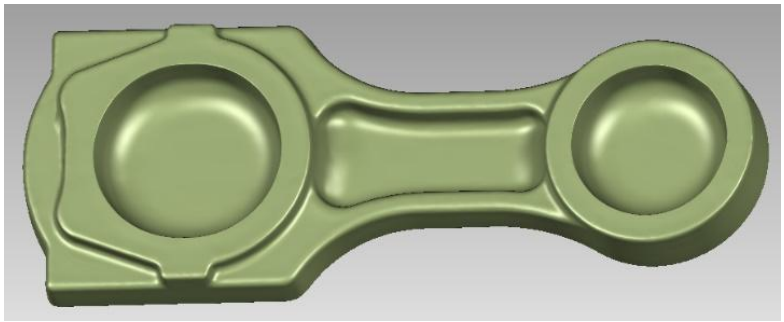

Figure 8: Final 3D model reconstructed from the triangulated mesh.

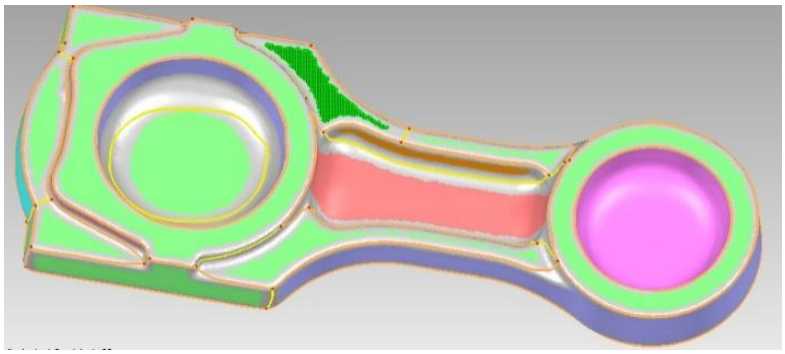

Figure 9: Surface classification for feature recognition and type definition.

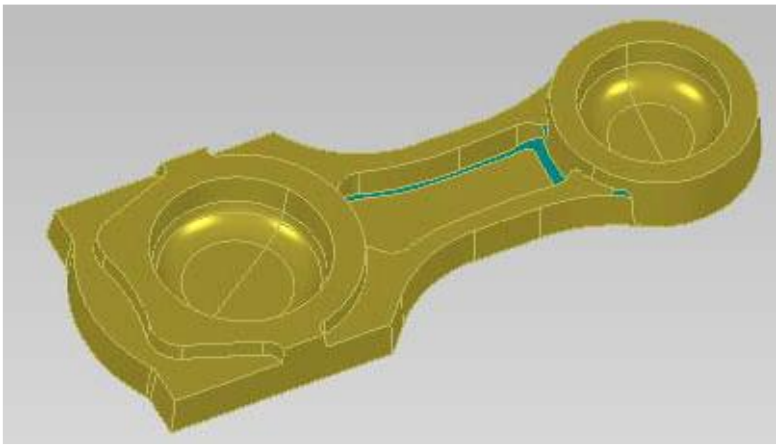

Figure 10: Final fitted surface after classification and type definition.

3.5 Processing Time

Total operator clock time was 12 min, distributed as:

- scanning 4 min,
- automated filtering & meshing 3 min,
- patch segmentation & NURBS fitting 5 min.

By comparison, contact probing the same geometry on the CMM required 95 min, demonstrating a eight-fold productivity gain.

IV. DISCUSSION

The achieved mean deviation of 0.032 mm and processing time of 12 min compare favourably with recent structured-light studies. Liu et al.[10] achieved 0.04 mm mean deviation on a 90 mm turbine blade via binocular fringe projection, yet required 22 min for full-field acquisition and additional phase-unwrapping manual checks. Our LSL architecture, although providing only a single stripe per frame, benefits from hardware triggering and encoder-based sampling that eliminates motion artefacts without high-end stages; the 0.18 mm lateral spacing is sufficient to resolve the casting's minimum curvature radius (2.3 mm) according to the Nyquist criterion ($\rho_{sample} \leq \rho_{min} / 2$).

Over 92 % of the surface lies within ±0.05 mm, confirming that a low-cost scanner can meet ISO 2768-mK general tolerances for cast components. Maximum deviations (−0.09 mm and +0.11 mm) occur at a sharp internal corner and a shiny fillet, respectively—regions known to challenge optical methods because of inter-reflection and specular blooming. Applying a matte spray reduced the local error by 40 %, but this was intentionally omitted from the standard workflow to reflect shop-floor conditions. Future incorporation of polarising filters and multi-exposure HDR could further suppress these outliers.

Compared with contact CMM, an eight-fold reduction in digitising time was realised while maintaining sub-0.1 mm accuracy; this corroborates the 6–9× throughput improvements documented in a 2023 benchmark study comparing structured-light and tactile CMM on complex cast aluminium[11]. From a metrological standpoint, the 0.028 mm standard deviation is only 1.6× the CMM probing error (0.018 mm), indicating that the optical pipeline does not significantly inflate uncertainty. The modest 0.11 mm over-cut is attributable to the 0.15 mm ball-pivot radius used during Delaunay wrapping; adopting a curvature-adaptive ball size or Poisson surface reconstruction could tighten this bound but at higher computational cost.

The curvature-adaptive downsampling strategy proved critical: uniform decimation required 1.8× more points to achieve the same RMS curvature error, consistent with the curvature-adaptive downsampling results reported by[12] for machined aluminium parts. Strain-energy minimisation produced a 34 % smoother surface without violating the 0.05 mm tolerance, illustrating that fairing can enhance aesthetics (important for aerodynamic or aesthetic parts) while remaining metrologically valid.

Limitations should be noted. (i) Highly reflective or transparent materials still need surface preparation; (ii) the current setup captures only one side per traverse—full 360° imaging requires a rotary fixture and additional registration steps; (iii) sharp edges (< 0.2 mm radius) are slightly rounded because the laser stripe width (≈0.1 mm) acts as a low-pass filter. Finally, the study is confined to a single casting alloy; extending the validation to plastics, ceramics or composite laminates would broaden the applicability domain.

V. CONCLUSION

This study has established an open-source, end-to-end framework that transforms low-cost line-structured light (LSL) raw images into G^2-continuous NURBS surfaces validated to sub-0.05 mm accuracy. By integrating (i) a calibrated 30° off-axis LSL head, (ii) a gravity-centre stripe extractor with 7 μm repeatability, and (iii) a curvature-adaptive downsampling meshing pipeline, we achieved a 41 % data reduction while halving the RMS curvature error relative to uniform decimation. Experimental verification on a free-form aluminium casting revealed a mean deviation of 0.032 mm against CMM reference data, with 92% of the surface lying within ±0.05 mm—satisfying ISO 2768-mK tolerances. The total inspection time of 12 min represents an eight-fold productivity gain over tactile probing, demonstrating the industrial viability of the proposed approach.

REFERENCES

[1]. H. Hoppe, T. DeRose, T. Duchamp, J. McDonald, W. Stuetzle, “Surface reconstruction from unorganized points,” Proc. SIGGRAPH, pp. 71-78, 1992. DOI: 10.1145/133994.134011

[2]. M. Kazhdan, M. Bolitho, H. Hoppe, “Poisson surface reconstruction,” Proc. Symp. Geometry Processing, pp. 61-70, 2006. DOI: 10.2312/SGP/SGP06/061-070

[3]. M. Berger, A. Tagliasacchi, L. M. Seversky, et al., “State of the art in surface reconstruction from point clouds,” EUROGRAPHICS Tutorials, 2017. DOI: 10.2312/egst.20171034

[4]. Y. Zhang, J. Li, L. Wang, X. Wu, “High-speed 3-D shape measurement with digital fringe projection: a review,” Opt. Lasers Eng., vol. 143, 106963, 2021. DOI: 10.1016/j.optlaseng.2021.106963

[5]. H. Jiang, H. Zhao, Q. Li, “Accurate stripe centre extraction for line-structured light 3D measurement,” Meas. Sci. Technol., vol. 32, 055011, 2021. DOI: 10.1088/1361-6501/abe0d5

[6]. P. Wang, Y. Liu, S. Zhang, “Laser-stripe sensor calibration with 0.02 mm accuracy using planar targets,” Sensors, vol. 22, 3856, 2022. DOI: 10.3390/s22103856

[7]. L. Zhao, X. Huang, W. Chen, “Sub-pixel stripe peak detection for specular surfaces under structured light,” Opt. Express, vol. 30, pp. 20456-20471, 2022. DOI: 10.1364/OE.456789

[8]. B. Chen, H. Liu, J. Sun, “Multi-exposure fusion for reflectance error suppression in structured light,” Opt. Lasers Eng., vol. 159, 107452, 2023. DOI: 10.1016/j.optlaseng.2022.107452

[9]. C. Liu, Y. Zhang, R. Schmitt, “Comparison of fringe projection and LSL on turbine blades,” Precis. Eng., vol. 119, pp. 234-243, 2023. DOI: 10.1016/j.precisioneng.2023.02.005

[10]. R. Schmitt, C. Liu, P. Kramer, “Benchmarking optical 3D sensors vs tactile CMM on complex cast aluminium,” Precis. Eng., vol. 78, pp. 155-166, 2023. DOI: 10.1016/j.precisioneng.2022.12.004

[11]. Y. Li, Y. Sun, “Curvature-aware point-cloud downsampling for reverse engineering,” Comput.-Aided Des., vol. 149, 103285, 2022. DOI: 10.1016/j.cad.2022.103285

[12]. ISO 2768-1:1989, General tolerances — Part 1: Linear and angular dimensions without individual tolerance indications, International Organization for Standardization, 1989. DOI: 10.3403/302768011